Non-Classical Behavior in Competitive Ion Adsorption at a Charged Solid–Water Interface

Sang Soo Lee[1*], Changyong Park[2], Neil C. Sturchio[3], and Paul Fenter[1]

[1] Chemical Sciences and Engineering Division, Argonne National Laboratory, 9700 South Cass Avenue, Lemont, IL 60439, United States

[2] HP-CAT, X-ray Science Division, Argonne National Laboratory, 9700 South Cass Avenue, Lemont, IL 60439, United States

[3] Department of Earth Sciences, University of Delaware, Newark, DE 19716, United States

[*]Corresponding author: phone: (630)252-6679; e-mail: sslee@anl.gov (S.S.L.)

ABSTRACT: Ion adsorption at solid-water interfaces is commonly described by interactions between specific surface sites and adsorbed ions in classical models. However, energetic contributions from non-site-specific ion-ion interactions have been less well understood. Here, we report non-classical behaviors observed during competitive adsorption between Sr^{2+} and Na^{+}/Rb^{+} at the negatively-charged muscovite mica (001)-water interface, revealing apparent controls of adsorbed ion speciation over the interfacial reactivity. In the absence of competing cations, Sr^{2+} adsorbs in approximately equivalent proportions of inner-sphere and outer-sphere complexes, whereas it adsorbs predominantly as an outer-sphere complex in the presence of Na^{+}/Rb^{+}. This transformation of adsorbed Sr^{2+} speciation significantly decreases its adsorption strength, as indicated by ~15-fold shift in the Sr^{2+} adsorption edge concentration, compared to that calculated from a classical Langmuir isotherm model developed based on site-specific interactions. These observations highlight the importance of non-site-specific interactions in controlling the energetics of chemical reactions at the charged interface.

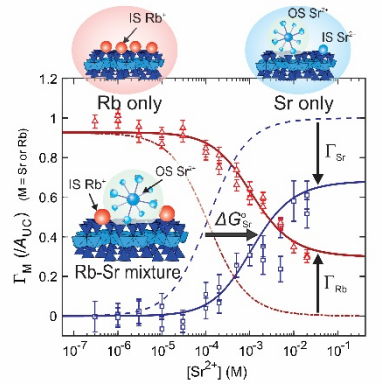

TOC Graphic

Solid–water interfaces are primary sites for a wide range of physicochemical phenomena. Adsorption and desorption of ions determine growth and dissolution of solids from aqueous solutions.[1-3] Sorption of heavy metals on mineral surfaces controls transport of toxic elements in aquifers and surface waters.[4-7]

Ion adsorption at a solid–water interface is normally described by chemical models based on a suite of elementary reactions defined by site-specific adsorption strength (i.e., affinity of an ion to a specific surface site) and capacity (i.e., a number of reactive sites available for ion adsorption).[8-11] Traditionally, these quantities are obtained from batch isotherm measurements, where variations in adsorbed ion coverage to model adsorbents (e.g., oxides or silicates) are recorded as a function of ion concentration, solution pH, and background electrolyte (BE) contents. Molecular insights into the site-specific reactions have been obtained mainly from spectroscopic studies.[5,12-15] Many adsorption models incorporate molecular-scale details of inner-sphere (IS) complexes that bind directly to surface ligands.[16] In contrast, the contribution from outer-sphere (OS) complexes, which adsorb on a surface in a fully hydrated state,[16] is estimated indirectly from changes in ion uptake as a function of BE concentration. However, there is growing evidence that electrostatic contributions of BE ions on the chemical binding of ions on a charged interface can be more complicated than they are generally assumed.[17-20] In addition, recent theoretical studies[21-24] predict the significant impacts of non-site-specific ion–ion interactions on the overall interfacial energetics, indicating the need for a more rigorous understanding of the adsorption processes at the atomic scale.

Here, we illustrate how the monovalent BE cations, Na^+ and Rb^+, alter the adsorption behavior of a divalent cation, Sr^{2+}, at the muscovite mica (001)–water interface in a manner that is not accounted for in classical adsorption models (e.g., competitive adsorption models using Langmuir-

type isotherm approaches). The (001) cleavage plane of muscovite mica is widely used as a model system for ion and molecule adsorption[18,25-30] because of its well-defined structure (composed of pseudo-hexagonal-lattice siloxane groups containing regularly-ordered ditrigonal cavities) and charge (~1e$^-$ per unit cell area, A_{UC} = 46.72 Å^2) at near-neutral pH.[31] Strontium was chosen as a target ion because of its well-known adsorption behavior on the mica surface. Previous studies using *in situ* resonant anomalous X-ray reflectivity (RAXR, Figure 1A) have shown that Sr^{2+} adsorbs in approximately equal proportions of IS and OS complexes over a wide range of $Sr(NO_3)_2$ and $SrCl_2$ concentrations (0.01–100 mM) in the absence of additional BE (Figure 1B).[25,32] Well-defined adsorption energetics for Sr^{2+} have also been reported in the studies (Table S1).

In this study, we quantify adsorption of Sr^{2+} on the mica surface in the presence of Rb^+ and Na^+, two BE cations that are commonly used because of their simple aqueous chemistry. These alkali metal cations show a clear difference in adsorption strength to the mica surface. For example, intrinsic adsorption constant for Rb^+, K^o_{Rb}, is significantly greater than K^o_{Na} ($10^{4.12\pm0.10}$ vs. $10^{2.51\pm0.14}$, corresponding to the intrinsic free energy of adsorption for Rb^+ and Na^+, ΔG^o_{Rb} = –23.5±0.6 kJ/mol and ΔG^o_{Na} = –14.3±0.8 kJ/mol, respectively; Table S1).[18,25] Rb^+ adsorbs on the mica surface predominantly as an IS complex in the ditrigonal cavity site (Figure 1C) whereas Na^+ is inferred to adsorb as an IS complex on top of the basal oxygen plane or an OS complex distributed farther from the surface.[18,28] Because of these well-known interfacial structures and properties, any deviations of the impact of these BE cations on Sr^{2+} adsorption beyond those calculated from classical competitive adsorption models can be directly evaluated and quantified to highlight the role of non-classical ion adsorption behavior at the charged mica interface.

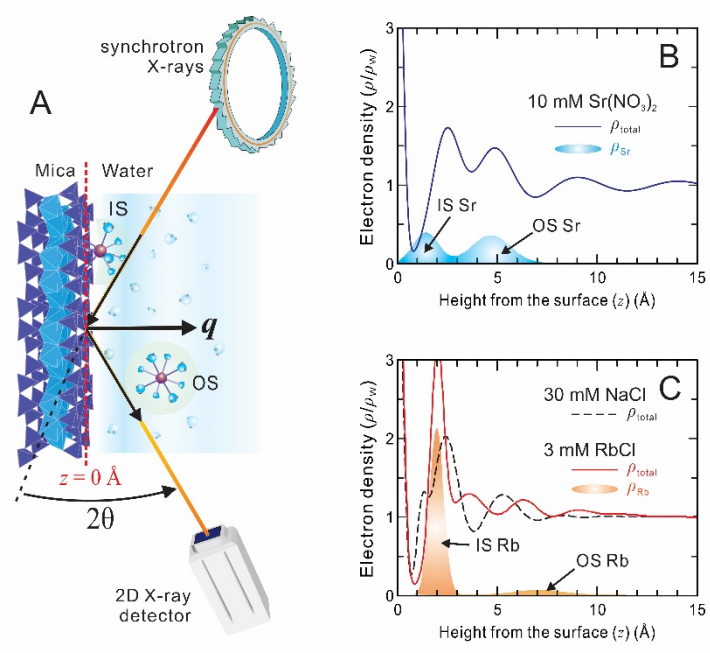

Figure 1. Adsorbed cation distribution at the muscovite mica (001)–water interface. (A) Schematic of an experimental setup for *in situ* resonant anomalous X-ray reflectivity (RAXR) measurements. Details of the experiment designs are shown in Figure S1. X-ray data are collected as a function of photon energy (E) at a fixed momentum transfer ($\boldsymbol{q}$) whose magnitude q is defined as $4\pi\sin(2\theta/2)/\lambda$ using the scattering angle (2θ) and X-ray wavelength ($\lambda = 12.4/E$). The analysis determines the distribution of adsorbed cations, including inner-sphere (IS) and outer-sphere (OS) complexes, as a function of height (z) from the top oxygen plane of the surface. (B and C) Interfacial structure between the muscovite mica (001) and solutions containing 10 mM $Sr(NO_3)_2$,[32,33] 30 mM NaCl and 3 mM RbCl.[34] The total electron-density profile (ρ_{total}) was determined from the high-resolution X-ray reflectivity (XR) analysis of each dataset. The distributions of IS and OS Sr^{2+} and Rb^{+}, respectively, were determined from the RAXR analysis.

Change in adsorption free energy of Sr at the mica–water interface. We first determined the effect of monovalent BE cations on the adsorption strength of Sr^{2+} to the muscovite mica (001)–water interface. Sr^{2+} adsorption isotherms were collected as a function of total Sr concentration in solution, [Sr], ranging from 0 to 20 mM, at a fixed concentration of NaCl (75 mM) and RbCl (3 mM). The higher concentration was used for Na^{+} to compensate for its weaker adsorption to the mica surface than Rb^{+}.[18,25] A simple calculation based on a site-specific two-component Langmuir isotherm (see Results for details) predicts that the two BEs should have a similar impact on Sr. In

both BE solutions, dissolved Sr species is expected to exist mostly (>90%) as Sr^{2+} with a minor fraction (up to ~8% in the NaCl solution) present as $SrCl^{+}$ (Figure S2).

The adsorbed Sr^{2+} coverage was measured using *in situ* RAXR. The data were collected near the Sr *K*-absorption edge energy (E_{Sr} = ~16.1 keV) at a fixed momentum transfer q = 0.48 $Å^{-1}$, an optimal scattering condition for determining the coverage and average height of Sr^{2+} adsorbed at the mica surface.[35] The deviation of a measured spectrum from the baseline intensity calculated based on the absence of interfacial Sr^{2+}—hereafter referred to as the RAXR signal—is proportional to the amount of Sr^{2+} adsorbed on the mica surface. Sr-RAXR signals in both BE solutions (i.e., 75 mM NaCl and 3 mM RbCl solutions) are generally smaller than those in $Sr(NO_3)_2$ solutions (without added BE) at the same [Sr], reflecting a decrease in Sr^{2+} coverage by competition with Na^{+} and Rb^{+} at the mica surface (Figures 2A–C, S3 and S4). Between the data collected in NaCl and RbCl solutions, the RAXR signals in RbCl solution generally are smaller than those in NaCl solution at the same [Sr], indicating the stronger influence of Rb^{+} on Sr^{2+} adsorption. The Rb^{+} effect was further corroborated by monitoring the evolution of adsorbed Rb^{+} distribution during Sr^{2+} uptake. The Rb-RAXR data were collected near the Rb *K*-absorption edge energy (E_{Rb} = ~15.2 keV) (Figures 2D and S4B). A systematic decrease in Rb-RAXR signal with increasing [Sr] reflects the replacement of Rb^{+} by Sr^{2+} at the interface (Figure 2D). However, the Rb signals never reached zero, even at [Sr] = 20 mM (i.e., the highest [Sr] applied in this study), indicating incomplete displacement at the interface. This is unexpected considering that the concentration of divalent Sr was significantly higher than that of monovalent Rb (i.e., [Sr] = 20 mM vs. [Rb] = 3 mM) and that divalent Sr is reported to adsorb more strongly to the negatively charged mica surface than monovalent Rb (e.g., K^{o}_{Sr} = ~$10^{5.7}$ vs. K^{o}_{Rb} = ~$10^{4.1}$).[25]

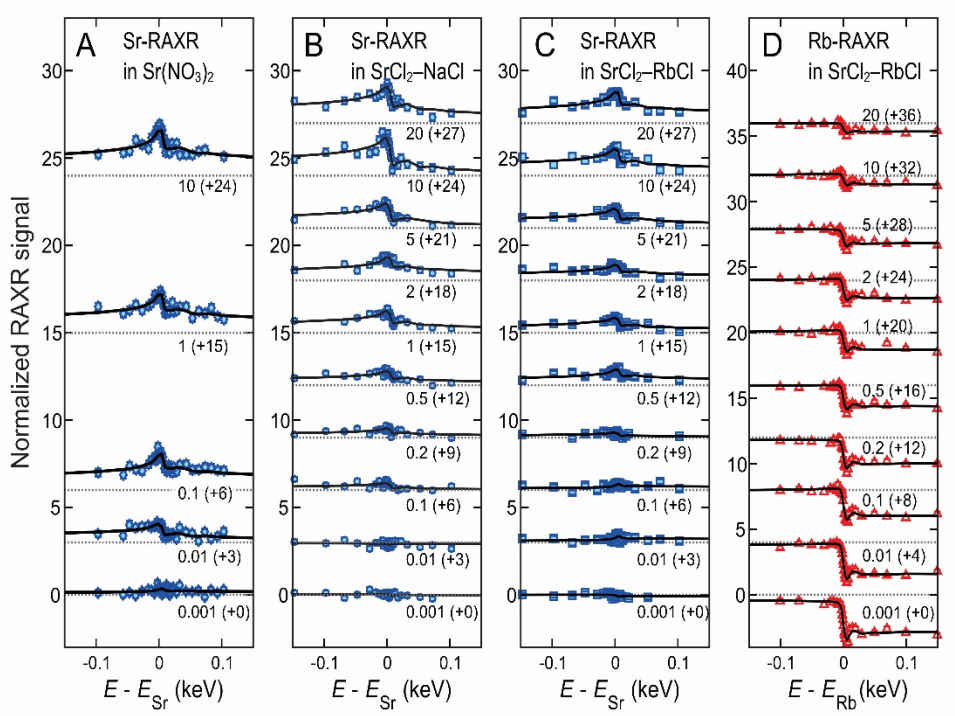

Figure 2. Effect of background electrolyte (BE) cations on the Sr^{2+} adsorption isotherm at the muscovite mica (001)–water interface. Resonant anomalous X-ray reflectivity data were collected as a function of aqueous Sr concentration, [Sr], near the *K*-absorption edge energy of Sr ($E_{Sr} \approx 16.1$ keV) in the absence of added BE[32] (A), in 75 mM NaCl (B) and in 3 mM RbCl (C), respectively. In the RbCl solution, a parallel set of data were collected near the *K*-absorption edge energy of Rb ($E_{Rb} \approx 15.2$ keV) (D) to monitor the change in adsorbed Rb^+ coverage as a function of [Sr]. Full datasets including the duplicates are shown in Figures S3 and S4. Each spectrum is labeled with [Sr] (in units of mM) and the magnitude of the vertical offset (in the parentheses) applied for visual comparison. The spectra are normalized based on the resonant amplitude normalization method $(|F_{tot}(q,E)|^2 - |F_{NR}(q)|^2)/(2|F_{NR}(q)|)$, where F_{tot} and F_{NR} are total and non-resonant structure factors, respectively[36]. Any significant differences of the measured spectra from the baseline intensity, shown as dotted horizontal lines, arise from adsorbed Sr (for A–C) and Rb (for D) species.

The non-classical response of Sr^{2+} uptake to the monovalent cation competition is illustrated by comparing the Sr^{2+} uptake isotherms (measured by RAXR) with those predicted with a classical isotherm model using the known adsorption constants of the individual cations on the mica surface.[18,25] This model calculation was conducted using a two-component Langmuir isotherm as

$$\Gamma_{Sr}([Sr]) = \Gamma_{Sr,max}\, a_{Sr}K^{o}_{Sr}/(1+a_{Sr}K^{o}_{Sr}+a_{BE}K^{o}_{BE}) \qquad (1)$$

where $\Gamma_{Sr}([Sr])$ is the total Sr^{2+} coverage at [Sr], $\Gamma_{Sr,max}$ is the maximum Sr^{2+} coverage on the mica surface (e.g., $\Gamma_{Sr,max}$ = ~0.5 Sr^{2+}/A_{UC} for Sr^{2+} to fully compensate the surface charge of mica, ~1 e^-/A_{UC}), a_{Sr} and a_{BE} are the activities of Sr^{2+} and a BE cation (i.e., Na^+ or Rb^+), respectively, in solution. K^o values are the intrinsic adsorption constants that have been determined for the individual cations in previous studies.[18,25,37]

The experimental data deviate significantly from theoretical expectations within the context of classical competitive adsorption models. The measured isotherms are shifted toward higher [Sr] (by ~one order of magnitude) with respect to the calculated curves (Figure 3), indicating that Sr^{2+} species adsorbs less strongly to the mica surface than predicted in the presence of the BE cations. Because the data were collected during the competitive adsorption between Sr^{2+} and the BE cations, it is not possible to determine whether the change was due to the decreased adsorption strength of Sr^{2+} or increased adsorption strength of the BE cations. Instead, the BE effect can be quantified by using the change in the adsorption free energy difference between Sr^{2+} and BE cations with respect to the theoretical value, defined as $\delta_{Sr–BE}$ where BE = Na and Rb, respectively.

The uptake data during competitive adsorption between Sr^{2+} and BE cations were analyzed using a modified two-component Langmuir isotherm expressed with the change in the adsorption free energy difference ($\delta_{Sr–BE}$) and maximum ion coverage ($\Gamma_{M,max}$ where M = Sr or Rb) (Table S2). The $\delta_{Sr–Na}$ value of 6.8±1.0 kJ/mol was obtained from the Sr^{2+} adsorption isotherm in 75 mM NaCl. The positive free energy indicates the decreased thermodynamic stability for Sr^{2+} adsorbed at the interface, whose magnitude corresponds to the amount of chemical shift of the Sr^{2+} absorption edge in the isotherm. The derived change in the adsorption constant for Sr^{2+} of $e^{6.8/RT}$ = ~15 (where R is the ideal gas constant and T is room temperature) matches the [Sr] shift observed in the uptake curve (Figure 3A). The derived $\Gamma_{Sr,max}$ value was 0.52±0.05 Sr^{2+}/A_{UC}, which is similar

to the amount of Sr^{2+} needed for full compensation of the negative charge of the mica surface (Table S2).

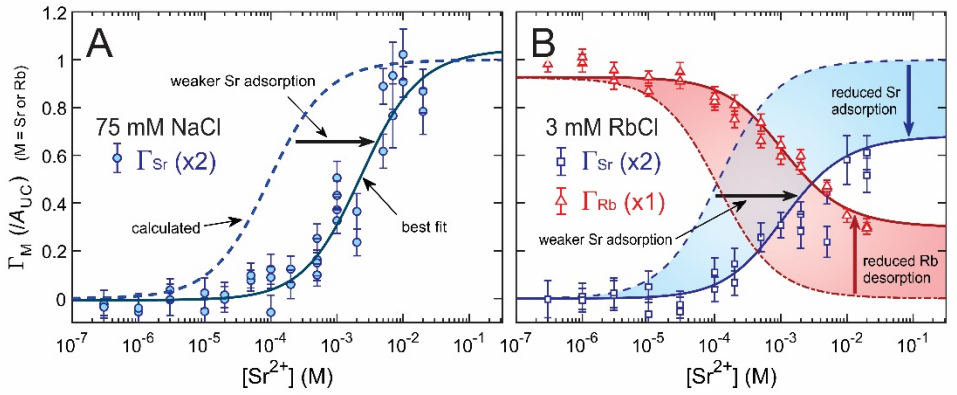

Figure 3. Sr^{2+} uptake isotherm on the muscovite mica (001) surface in 75 mM NaCl (A) and 3 mM RbCl (B). The dashed and dot-dashed curves were calculated based on the two-component Langmuir isotherm using the intrinsic adsorption constants for individual cations for Sr^{2+} and Rb^{+}, respectively (equation 1). The solid curves are the best fit to the data (Table S2).

The effect of Rb^{+} on Sr^{2+} uptake at the mica surface was different from that of Na^{+}. While the uptake curve shows a similar shift in Sr^{2+} adsorption edge, as evidenced by the similar δ_{Sr-Rb} value to δ_{Sr-Na} (5.6±1.9 and 6.8±1.0 kJ/mol, respectively, Table S2), it never reaches the theoretical maximum (~0.5 Sr^{2+}/A_{UC}) for the surface charge compensation up to the highest [Sr] (20 mM) used in the study. Instead, the analysis indicates that the uptake data are best described with a decreased maximum coverage, $\Gamma_{Sr,max}$ = 0.34±0.03 Sr^{2+}/A_{UC}, which is only ~2/3 the amount of Sr^{2+} required for full charge compensation. This estimated limitation in Sr^{2+} uptake is consistent with the incomplete replacement of Rb^{+} by Sr^{2+} at the surface even when [Sr] >> [Rb]. A significant amount of Rb^{+} (0.30±0.05 Rb^{+}/A_{UC}) remained adsorbed at the interface at higher [Sr] (Figure 3B). Nevertheless, the adsorbed coverages of Sr^{2+} and Rb^{+}, in total, are consistent with the amount needed to compensate the surface charge of the mica (i.e., compensating 0.98±0.08 e^{-}/A_{UC} of

surface charge vs. the nominal value of $1e^{-}/A_{UC}$ for the mica, with the assumption that adsorbed Sr was in the form of Sr^{2+}).

Changes in adsorbed Sr speciation by background electrolyte. We explore the possibility that the decrease of Sr^{2+} adsorption in the presence of the competing BE cations is controlled by changes in adsorbed Sr^{2+} speciation, such as a change in fractionation between IS and OS complexes or the formation of a new adsorbed species. *In situ* RAXR measurements were performed in 20 mM $SrCl_2$ solutions with 75 mM NaCl and 3 mM RbCl BE, respectively (Figures S5–S8) to probe the distributions of Sr^{2+} (and Rb^{+} for the latter) adsorbed on the mica surface as a function of height (z where z = 0 Å corresponds to the top oxygen plane of the mica surface).

The derived electron-density profiles show significant changes in adsorbed Sr^{2+} speciation by the BE cations (Tables S3–S6). The coexistence of three distinct Sr^{2+} species is observed on the mica surface in 20 mM $SrCl_2$ with 75 mM NaCl. Two of these species, located at z = 1.5 ± 0.1 Å and 4.7 ± 0.1 Å match the IS Sr^{2+} complex adsorbed in the ditrigonal cavity site and the OS Sr^{2+} complex adsorbed on top of the surface oxygen plane, respectively, that were determined previously in NaCl-free solution (Figure 4A),[32,33] but with reduced coverages (by 41 and 31%, respectively) (Table 1). The profile also contains a third species that is distributed farther from the surface (around z = 8.5 ± 0.2 Å). The total coverage of Sr^{2+} over the three species is 0.48 ± 0.03 Sr^{2+}/A_{UC}, which is slightly smaller than the coverage measured without added BE cations (Table 1), but consistent with full charge compensation by a divalent cation (0.5 Sr^{2+}/A_{UC} for $1e^{-}/A_{UC}$ of the surface charge).[31]

Changes in adsorbed Sr^{2+} speciation were more pronounced with 3 mM RbCl. Inner-sphere Sr^{2+} shows a significant reduction in coverage (89%) whereas OS Sr^{2+} shows a smaller reduction (39%, Table 1). These observations indicate that the presence of Rb^{+} preferentially destabilizes IS

Sr^{2+} to OS Sr^{2+}. The decreased coverage is partially balanced with Sr^{2+} adsorbing farther from the surface (Figure 4B). The overall coverage of Sr^{2+} adsorbed on the mica surface is 0.31±0.02 Sr^{2+}/A_{UC}, which is 46% lower than that measured without RbCl (Table 1) and ~40% lower than the amount needed for satisfying the surface charge of mica. The remaining surface charge is compensated by Rb^+ whose total coverage is 0.46±0.02 Rb^+/A_{UC}, which is roughly half of Rb^+ coverage observed in pure 3 mM RbCl solution. Even in the presence of Sr^{2+}, most of Rb^+ adsorption occurs as an IS species at z = 2.06±0.02 Å, similar to that in the Sr-free solution (Figure 4B).

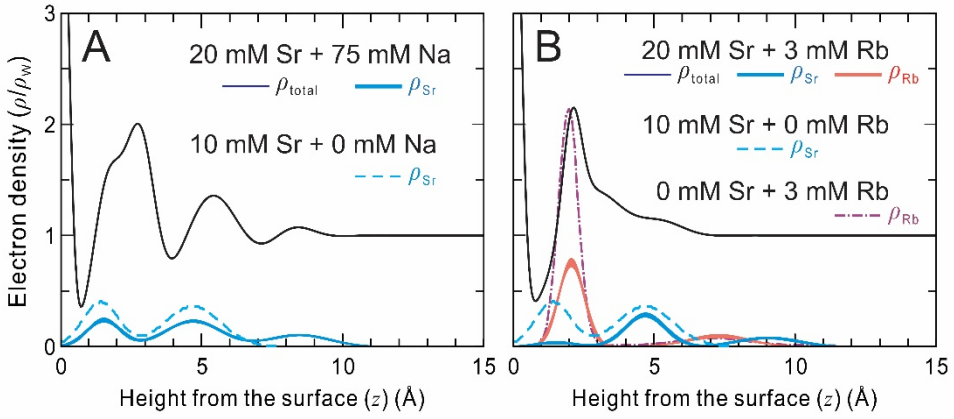

Figure 4. Distributions of Sr^{2+} adsorbed at the muscovite mica (001)–20 mM $SrCl_2$ solution interface in 75 mM NaCl and 3 mM RbCl BE, respectively. (A) Interfacial electron-density profile between the mica (001) and 20 mM $SrCl_2$ solution with 75 mM NaCl BE. The total electron-density profile (ρ_{total}) and the Sr^{2+} electron-density profile (ρ_{Sr}) were derived from the XR and RAXR data analyses, respectively (Figures S5–S8 and Tables S3–S6). The ρ_{Sr} derived from the RAXR data measured at the mica (001)–10 mM $Sr(NO_3)_2$ solution interface without added BE[32,33] is also shown for comparison. (B) Interfacial electron-density profile between the mica (001)–20 mM $SrCl_2$ solution with 3 mM RbCl BE. The ρ_{total} was derived from the XR data analyses. The electron-density profiles of Sr^{2+} and Rb^+ (ρ_{Sr} and ρ_{Rb}, respectively) were derived from the RAXR data analyses. The ρ_{Sr} derived from 10 mM $Sr(NO_3)_2$ solution[32,33] and the ρ_{Rb} derived from 3 mM RbCl solution[34] are also shown for comparison. The ρ_{total} measured in the $Sr(NO_3)_2$ solution and that in the RbCl solution are shown in Figures 1B and C, respectively. The electron density is normalized to that of bulk water (ρ_W). The height is calculated from the top oxygen plane of the mica surface (z = 0 Å).

Table 1. The effect of BE cations, Na^+ and Rb^+, on the coverages of individual Sr^{2+} species adsorbed at the muscovite mica (001)–water interface.

Solutions	Adsorbed Sr^{2+} Coverages [a]			
	$\Gamma_{Sr,IS}$	$\Gamma_{Sr,OS1}$	$\Gamma_{Sr,OS2}$	Γ_{Sr}
10 mM $Sr(NO_3)_2$ without BE [b]	0.24 ± 0.02	0.33 ± 0.02	nd [c]	0.57 ± 0.03
20 mM $SrCl_2$ in 75 mM NaCl BE	0.14 ± 0.01 (–41%) [d]	0.23 ± 0.01 (–31%) [d]	0.11 ± 0.01	0.48 ± 0.02 (–16%) [d]
20 mM $SrCl_2$ in 3 mM RbCl BE	0.03 ± 0.01 (–89%) [d]	0.20 ± 0.01 (–39%) [d]	0.08 ± 0.01	0.31 ± 0.02 (–46%) [d]

[a] $\Gamma_{Sr,IS}$, $\Gamma_{Sr,OS1}$, and $\Gamma_{Sr,OS2}$: adsorbed coverages of inner-sphere (IS) Sr^{2+} adsorbed at ~1.5 Å and two outer-sphere (OS) Sr^{2+} (1 and 2) adsorbed at ~4.7 and ~8.5–9.0 Å, respectively. See Figure 4 for details. Γ_{Sr}: the total coverage of all adsorbed Sr^{2+} species. The coverages are expressed in units of Sr^{2+}/A_{UC}.

[b] Refs.[32,33]

[c] not detected

[d] The fractional changes in coverage with respect to those without BE are shown in the parentheses.

Our experimental observations show that monovalent Na^+ and Rb^+ modify the speciation and energetics of divalent Sr^{2+} adsorbed on the negatively charged basal surface of muscovite mica. In the absence of additional BE, Sr^{2+} adsorbs in equal proportions of IS and OS complexes from a 10 mM $Sr(NO_3)_2$ solution.[32,33] Competition with monovalent BE cations generally leads to transformation of the Sr^{2+} adsorption to OS-dominant adsorption, including a new Sr^{2+} species distributed farther from the surface than the previously observed IS and OS Sr^{2+} species (Figure 4). This change in adsorbed cation speciation effectively increases the average distance between the cation and the negatively charged surface, which thereby decreases electrostatic attraction between the adsorbate and the adsorbent, consistent with the decrease in adsorption free energy of Sr^{2+} by the BE cations from the uptake isotherm measurements.

The detailed changes in the adsorbed Sr^{2+} speciation are controlled by the properties of competing monovalent cations. The influence of Na^+ on IS and OS Sr^{2+} species was approximately equal, which is largely consistent with the behavior expected for ions adsorbed on a surface by a non-site-specific interaction (e.g., mean-field interactions between ions within the electrical double layer)[16] although the development of a third Sr^{2+} species adsorbed farther from the surface is not explained by this simple picture. In contrast, the preferential impact of Rb^+ on IS Sr^{2+} over OS Sr^{2+} agrees with the behavior expected from the classical competitive adsorption model for specific surface sites (i.e., ditrigonal cavity sites on the muscovite mica (001) plane)[28,30,32,38-40]. Inner-sphere adsorption of Sr^{2+} can be hindered by direct competition with IS Rb^+ for the same surface sites. In comparison, such site-specific effect was less pronounced in the NaCl BE, consistent with the previous observation that only a portion of adsorbed Na^+ formed an IS complex on the mica surface.[18,28] For both Rb^+ and Na^+, the BE impact on OS Sr^{2+} was relatively small, indicating the site-specific competition between these adsorbed species was also small.

While competitive adsorption between IS Sr^{2+} and IS Rb^+ can explain the decreased adsorption of IS Sr^{2+}, it cannot explain the incomplete exchange of Rb^+ by Sr^{2+} observed at elevated [Sr] (up to 20 mM). Adsorption of Sr^{2+} and Rb^+ on the mica surface is controlled by simple electrostatic attraction, thus it is expected that divalent Sr^{2+} should readily outcompete monovalent Rb^+. However, both the uptake isotherm and the structure measurements show a significant fraction of Rb^+ remaining at the interface even when [Sr] is significantly higher than [Rb]. We confirmed that this incomplete substitution was not controlled by reaction kinetics as we achieved fully reversible exchange between Rb^+ and Sr^{2+} within far shorter reaction time ($<<$ 1 min)[41] than the equilibration time ($\geq$5 min) applied for each step. Therefore, we conclude that the coexistence between IS Rb^+

and OS Sr^{2+} is an equilibrium phenomenon that occurs at the charged mica–water interface in the mixed solution composition.

We speculate that the observed structure can be stabilized by the local coordination of cations adsorbed at the mica surface.[21-22] The interfacial structure observed during the competition between Rb^+ and Sr^{2+} cannot be expressed by a simple linear combination of those in pure Rb and pure Sr solutions[32,34] (Figure 5), which, again, is attributed in part to the direct competition between IS Rb^+ and IS Sr^{2+} for the specific surface sites. In contrast, OS Sr^{2+} species are spatially less constrained and thereby they can be more readily distributed to maximize the distance between Rb^+ and Sr^{2+} and effectively minimize the electrostatic repulsion between the adsorbates.[23-24]

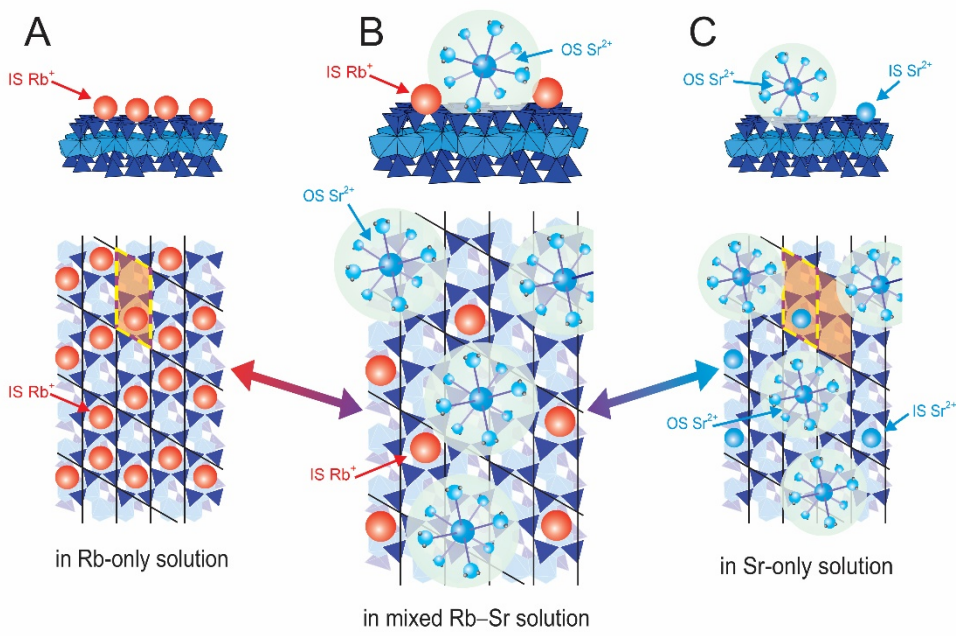

Figure 5. Schematic of distribution of mixed states of Rb^+ and Sr^{2+} adsorbed on the muscovite mica surface inferred from X-ray measurements. (A) and (C) the equilibrium distribution of Rb^+ and Sr^{2+} adsorbed on the muscovite mica (001)–3 mM RbCl and 10 mM $Sr(NO_3)_2$ solution interfaces, respectively.[32,34] The hydration structure around the IS species is omitted for the clarity. In 3 mM RbCl, a minor fraction of Rb^+ (<10%) also adsorbs as an OS species (not shown). (B) Coexistence of IS Rb^+ and OS Sr^{2+} adsorbed on the mica surface from a 20 mM $SrCl_2$ and 3 mM RbCl solution. The lateral distribution of the adsorbates is inferred from the X-ray reflectivity data to simulate the strong positional

correlation expected at the highly charged mica surface. The second OS Sr^{2+} adsorbed farther from the surface (i.e., 7–11 Å from the mica surface) is not presented for simplicity. The arrow between (A) and (B) indicates the series of solution composition used in our uptake experiments (Figure 2).

We infer that this exchange process can be spontaneous with increasing [Sr] until the system reaches a maximum Sr^{2+} coverage at which all adsorbed Sr^{2+} are fully coordinated with Rb^{+} as their nearest neighboring cations. Ideally, this local saturation occurs when Sr^{2+} and Rb^{+} coverages are approximately equal to each other (Figure 5B), which, interestingly, is very close to the equilibrium elemental composition of the interface measured by our X-ray data (Figure 3B). This inferred 2D arrangement, although it has yet to be measured directly, resembles a Wigner crystal structure, which can be stabilized via strong ion–ion correlations at highly charged interfaces.[19-22] However, this theoretical structure is presumably too simple to represent the actual structure at the mica–water interface. In particular, interfacial water is expected to play a critical role in stabilizing the adsorbed cation distribution. The proximity between partially hydrated IS Rb^{+} and fully hydrated OS Sr^{2+} can result in partial overlap between their solvation shells, in which the water molecules continuously change their positions[42] and dynamically distort the coordination environments around the adsorbed cations. The arrangement of IS Rb^{+} and OS Sr^{2+} can also be affected by the lateral charge distribution within the mica surface. The negative charge on the muscovite mica surface originates from the isomorphic substitution of Al^{3+} for Si^{4+} in the tetrahedral sites.[38] Each ditrigonal cavity site, surrounded by six $(Si/Al)O_4$ tetrahedra, can have a different negative charge depending on the number of Al^{3+}-substitutions in the surrounding tetrahedra. This inhomogeneous distribution of the surface charge can influence the local cation distribution, which likely is more complex than depicted in the simple model.

The *in situ* observations of the structure and energetics of cations adsorbed on the negatively charged mica surface illustrate non-classical behavior that is controlled by complex chemical and

physical properties of the adsorbates at the interface. The unexpected decrease of the relative adsorption strength of Sr^{2+} on the mica surface can be explained by the changes in adsorbed Sr^{2+} speciation at the interface that strongly depend on the type of competing cation. The almost equal influence of Na^{+} on both Sr^{2+} species is largely consistent with a behavior expected for ions adsorbed on a surface by a non-specific interaction. In contrast, preferred desorption of IS Sr^{2+} over OS Sr^{2+} by Rb^{+} is likely controlled by site-specific competition, consistent with the basis for classical chemical complexation models. In both cases, additional stabilization of OS Sr^{2+} was observed farther from the surface, which cannot be explained by classical adsorption models that implicitly assume that OS species would be readily displaced by BE cations. In the RbCl solution with elevated [Sr], we observed coexistence between IS Rb^{+} and OS Sr^{2+}, which is proposed to be stabilized by the strong electrostatic correlations between the adsorbates near the highly charged mica surface. The consistency between this picture of mixed ion organization, theoretical prediction,[21-24] and our experimental data highlights the importance of the positional correlations over stabilization of competing cations adsorbed at the charged mica–water interface. The collective effects between site-specific and non-site-specific interactions at the interface have yet to be fully incorporated in modern chemical complexation models. We speculate that this non-classical behavior may also be important for other mineral–water interfacial systems, especially for those that exhibit high charge densities, including oxides, hydroxides, and other silicates, where ion adsorption is controlled by a combination of the intrinsic structural charge (similar to muscovite mica) and the pH-dependent charge of surface ligands.[8-11]

Associated content

Supporting information is available free of charge at https://pubs.acs.org/.

Materials and Methods, schematics of sample cells, thermodynamic calculation of solution Sr species, X-ray data and details of theoretical calculations and X-ray data analysis.

Author Information

Corresponding Author

Sang Soo Lee – *Chemical Sciences and Engineering Division, Argonne National Laboratory, 9700 South Cass Avenue, Lemont, IL 60439, United States;* orcid.org/0000-0001-8585-474X; Email: sslee@anl.gov

Authors

Changyong Park – *HP-CAT, X-ray Science Division, Argonne National Laboratory, 9700 South Cass Avenue, Lemont, IL 60439, United States;* orcid.org/0000-0002-3363-5788

Neil C. Sturchio – *Department of Earth Sciences, University of Delaware, Newark, DE 19716, United States;* orcid.org/0000-0002-7581-9585

Paul Fenter – *Chemical Sciences and Engineering Division, Argonne National Laboratory, 9700 South Cass Avenue, Lemont, IL 60439, United States;* orcid.org/0000-0002-6672-9748

Acknowledgments

This work was supported by U.S. Department of Energy, Office of Science, Office of Basic Energy Sciences, Chemical Sciences, Geosciences, and Biosciences Division under Contracts DE-AC02-06CH11357 to UChicago Argonne, LLC as operator of Argonne National Laboratory. C.P. acknowledges HPCAT, supported by DOE-NNSA's Office of Experimental Sciences. The X-ray data were collected at the beamline 6-ID-B, Advanced Photon Source. Use of the Advanced Photon Source was supported by the U.S. Department of Energy, Office of Science, Office of Basic Energy Sciences, under Contract DE-AC02-06CH11357 to UChicago Argonne, LLC as operator of Argonne National Laboratory. The submitted manuscript has been created by UChicago Argonne, LLC, Operator of Argonne National Laboratory ("Argonne"). Argonne, a U.S. Department of Energy Office of Science laboratory, is operated under Contract No. DE-AC02-06CH11357. The U.S. Government retains for itself, and others acting on its behalf, a paid-up nonexclusive, irrevocable worldwide license in said article to reproduce, prepare derivative works, distribute copies to the public, and perform publicly and display publicly, by or on behalf of the Government.

References

(1) Dove, P. M.; Han, N.; Yoreo, J. D. Mechanisms of classical crystal growth theory explain quartz and silicate dissolution behavior. *Proc. Natl. Acad. Sci. USA* **2005,** *102*, 15357-15362.

(2) Stack, A. G.; Raiteri, P.; Gale, J. D. Accurate rates of the complex mechanisms for growth and dissolution of minerals using a combination of rare-event theories. *J. Am. Chem. Soc. Comm.* **2012,** *134*, 11-14.

(3) Putnis, A. Why Mineral Interfaces Matter. *Science* **2014,** *343*, 1441-1442.

(4) Brown, G. E., Jr.; Foster, A. L.; Ostergren, J. D. Mineral surfaces and bioavailability of heavy metals: A molecular-scale perspective. *Proc. Natl. Acad. Sci. USA* **1999,** *96*, 3388-3395.

(5) Brown, G. E., Jr.; Henrich, V. E.; Casey, W. H.; Clark, D. L.; Eggleston, C.; Felmy, A.; Goodman, D. W.; Grätzel, M.; Maciel, G.; McCarthy, M. I.; Nealson, K. H.; Sverjensky, D. A.; Toney, M. F.; Zachara, J. M. Metal oxide surfaces and their interactions with aqueous solutions and microbial organisms. *Chem. Rev.* **1999,** *99*, 77-174.

(6) Steefel, C. I.; DePaolo, D. J.; Lichtner, P. C. Reactive transport modeling: An essential tool and a new research approach for the Earth sciences. *Earth Planet. Sci. Lett.* **2005,** *240*, 539-558.

(7) Maher, K.; Mayer, K. U. Tracking diverse minerals, hungry organisms, and dangerous contaminants using reactive transport models. *Elements* **2019,** *15*, 81-86.

(8) Sverjensky, D. A. Physical surface-complexation models for sorption at the mineral-water interface. *Nature* **1993,** *364*, 776-780.

(9) Hiemstra, T.; Van Riemsdijk, W. H. A surface structural approach to ion adsorption: The charge distribution (CD) model. *J. Colloid Interface Sci.* **1996,** *179*, 488-508.

(10) Rahnemaie, R.; Hiemstra, T.; van Riemsdijk, W. H. Inner- and outer-sphere complexation of ions at the goethite-solution interface. *J. Colloid Interface Sci.* **2006,** *297*, 379-388.

(11) Fukushi, K.; Sverjensky, D. A. A surface complexation model for sulfate and selenate on iron oxides consistent with spectroscopic and theoretical molecular evidence. *Geochim. Cosmochim. Acta* **2007,** *71*, 1-24.

(12) Hayes, K. F.; Roe, A. L.; Brown, G. E., Jr.; Hodgson, K. O.; Leckie, J. O.; Parks, G. A. In situ X-ray absorption study of surface complexes: Selenium oxyanions on α-FeOOH. *Science* **1987,** *238*, 783-786.

(13) Manceau, A.; Boisset, M.-C.; Sarret, G.; Hazemann, J.-L.; Mench, M.; Cambier, P.; Prost, R. Direct determination of lead speciation in contaminated soils by EXAFS spectroscopy. *Environ. Sci. Technol.* **1996,** *30*, 1540-1552.

(14) Venema, P.; Hiemstra, T.; van Riemsdijk, W. H. Multisite adsorption of cadmium on goethite. *J. Colloid Interface Sci.* **1996,** *183*, 515-527.

(15) Peacock, C. L.; Sherman, D. M. Copper(II) sorption onto goethite, hematite, and lepidocrocite: A surface complexation model based on ab initio molecular geometries and EXAFS spectroscopy. *Geochim. Cosmochim. Acta* **2004,** *68*, 2623-2637.

(16) Stumm, W.; Morgan, J. J. *Aquatic Chemistry*. 3rd ed.; John Wiley and Sons: New York, 1996.

(17) Catalano, J. G.; Park, C.; Fenter, P.; Zhang, Z. Simultaneous inner- and outer-sphere arsenate adsorption on corundum and hematite. *Geochim. Cosmochim. Acta* **2008,** *72*, 1986-2004.

(18) Lee, S. S.; Fenter, P.; Nagy, K. L.; Sturchio, N. C. Changes in adsorption free energy and speciation during competitive adsorption between monovalent cations at the muscovite (001)-water interface. *Geochim. Cosmochim. Acta* **2013,** *123*, 416-426.

(19) Laanait, N.; Mihaylov, M.; Hou, B.; Yu, H.; Vanýsek, P.; Meron, M.; Lin, B.; Benjamin, I.; Schlossman, M. L. Tuning ion correlations at an electrified soft interface. *Proc. Natl. Acad. Sci. USA* **2012,** *109*, 20326-20331.

(20) Lee, S. S.; Schmidt, M.; Laanait, N.; Sturchio, N. C.; Fenter, P. Investigation of adsorbed structure, adsorption free energy, and overcharging behavior of trivalent yttrium at the muscovite (001)-water interface. *J. Phys. Chem. C* **2013,** *117*, 23738-23749.

(21) Shklovskii, B. I. Screening of a macroion by multivalent ions: Correlation-induced inversion of charge. *Phys. Rev. E* **1999,** *60*, 5802-5811.

(22) Levin, Y. Electrostatic correlations: From plasma to biology. *Rep. Prog. Phys.* **2002,** *65*, 1577-1632.

(23) Lyklema, J. Quest for ion-ion correlations in electric double layers and overcharging phenomena. *Adv. Colloid Interface Sci.* **2009,** *147-48*, 205-213.

(24) Kjellander, R. Intricate coupling between ion-ion and ion-surface correlations in double layers as illustrated by charge inversion-combined effects of strong Coulomb correlations and excluded volume. *J. Phys.-Condes. Matter* **2009,** *21*, 16.

(25) Park, C.; Fenter, P. A.; Sturchio, N. C.; Nagy, K. L. Thermodynamics, interfacial structure, and pH hysteresis of Rb^+ and Sr^{2+} adsorption at the muscovite (001)-solution interface. *Langmuir* **2008,** *24*, 13993-14004.

(26) Ricci, M.; Spijker, P.; Voïtchovsky, K. Water-induced correlation between single ions imaged at the solid-liquid interface. *Nat. Commun.* **2014,** *5*, 4400.

(27) Martin-Jimenez, D.; Chacon, E.; Tarazona, P.; Garcia, R. Atomically resolved three-dimensional structures of electrolyte aqueous solutions near a solid surface. *Nat. Commun.* **2016,** *7*, 7.

(28) Bourg, I. C.; Lee, S. S.; Fenter, P.; Tournassat, C. Stern layer structure and energetics at mica–water interfaces. *J. Phys. Chem. C* **2017,** *121*, 9402-9412.

(29) Ricci, M.; Trewby, W.; Cafolla, C.; Voitchovsky, K. Direct observation of the dynamics of single metal ions at the interface with solids in aqueous solutions. *Sci Rep* **2017,** *7*, 12.

(30) Adapa, S.; Malani, A. Role of hydration energy and co-ions association on monovalent and divalent cations adsorption at mica-aqueous interface. *Sci Rep* **2018,** *8*, 12.

(31) Schlegel, M. L.; Nagy, K. L.; Fenter, P.; Cheng, L.; Sturchio, N. C.; Jacobsen, S. D. Cation sorption on the muscovite (001) surface in chloride solutions using high-resolution X-ray reflectivity. *Geochim. Cosmochim. Acta* **2006,** *70*, 3549-3565.

(32) Park, C.; Fenter, P. A.; Nagy, K. L.; Sturchio, N. C. Hydration and distribution of ions at the mica-water interface. *Phys. Rev. Lett.* **2006,** *97*, 016101-1-4.

(33) Lee, S. S.; Park, C.; Fenter, P.; Sturchio, N. C.; Nagy, K. L. Competitive adsorption of strontium and fulvic acid at the muscovite-solution interface observed with resonant anomalous X-ray reflectivity. *Geochim. Cosmochim. Acta* **2010,** *74*, 1762-1776.

(34) Lee, S. S.; Fenter, P.; Nagy, K. L.; Sturchio, N. C. Monovalent ion adsorption at the muscovite (001) - solution interface: Relationships among ion coverage and speciation, interfacial water structure, and substrate relaxation. *Langmuir* **2012,** *28*, 8637-8650.

(35) Park, C.; Fenter, P. A. Phasing of resonant anomalous X-ray reflectivity spectra and direct Fourier synthesis of element-specific partial structures at buried interfaces. *J. Appl. Crystallogr.* **2007,** *40*, 290-301.

(36) Lee, S. S.; Nagy, K. L.; Park, C.; Fenter, P. Enhanced uptake and modified distribution of mercury(II) by fulvic acid on the muscovite (001) surface. *Environ. Sci. Technol.* **2009,** *43*, 5295-5300.

(37) Lee, S. S.; Fenter, P.; Nagy, K. L.; Sturchio, N. C. Real-time observation of cation exchange kinetics and dynamics at the muscovite–water interface. *Nat. Commun.* **2017,** *8*, 15826.

(38) Bailey, S. W. *Micas*. The Mineralogical Society of America: Washington, DC, 1984; Vol. 13, p 584.

(39) Meleshyn, A. Adsorption of Sr^{2+} and Ba^{2+} at the cleaved mica-water interface: Free energy profiles and interfacial structure. *Geochim. Cosmochim. Acta* **2010,** *74*, 1485-1497.

(40) Pintea, S.; de Poel, W.; de Jong, A. E. F.; Vonk, V.; van der Asdonk, P.; Drnec, J.; Balmes, O.; Isern, H.; Dufrane, T.; Felici, R.; Vlieg, E. Solid–liquid interface structure of muscovite mica in CsCl and RbBr solutions. *Langmuir* **2016,** *32*, 12955-12965.

(41) Lee, S. S.; Fenter, P.; Park, C. Optimizing a flow-through X-ray transmission cell for studies of temporal and spatial variations of ion distributions at mineral-water interfaces. *J. Synchrotron Radiat.* **2013,** *20*, 125-136.

(42) Lincoln, S. F. Mechanistic studies of metal aqua ions: A semi-historical perspective. *Helv. Chim. Acta*, **2005,** *88*, 523-545.